Journal of Hydrology: Regional Studies 54 (2024) 101879

Contents lists available at ScienceDirect

Journal of Hydrology: Regional Studies

journal homepage: www.elsevier.com/locate/ejrh

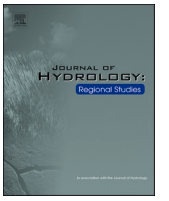

Downscaling and validating GLDAS groundwater storage anomalies by integrating precipitation for recharge and actual evapotranspiration for discharge

Cindy Viviers [a,*,1], Michael van der Laan [a,b,2], Zaheed Gaffoor [c], Matthys Dippenaar [d,3]

[a] Department of Plant and Soil Sciences, University of Pretoria, Pretoria 0028, South Africa
[b] Agricultural Research Council – Natural Resources and Engineering, Pretoria 0001, South Africa
[c] IBM Research Africa, Johannesburg 2001, South Africa
[d] Department of Geology, University of Pretoria, Pretoria 0028, South Africa

ARTICLE INFO

Keywords:
CHIRPS precipitation
MOD16 ET_a
Remote and satellite sensing
Machine learning
South Africa

ABSTRACT

Study region: The Steenkoppies Catchment is located approximately 75 km southwest from Pretoria, South Africa (RSA).
Study focus: This study tested a framework for downscaling Global Land Data Assimilation System (GLDAS-2.2) groundwater storage anomaly (GWSA) estimates from 0.25° to 0.05°. This was achieved in Google Earth Engine using the Random Forest algorithm with only precipitation and actual evapotranspiration (ET_a) as input variables. Additionally, the study assessed whether accounting for temporal lags could minimise residuals and enhance model performance.
New hydrological insights for the region: The greater range of downscaled GWSA values indicated that the product effectively captured local recharge (precipitation) and discharge (ET_a) variations while maintaining conservation of mass. Optimising the temporal correlation (*r*) between input variables resulted in lower residuals and fewer outliers. Groundwater level measurements and downscaled estimates for the hard rock aquifer showed larger amplitudes and seasonality and yielded the highest *r* (0.6) and lowest RMSE (40 mm) and MAE (31 mm). Measurements near the spring and in the karst aquifer showed less evident amplitude and seasonality. The *in situ* derived and downscaled GWSA comparison demonstrated the effectiveness of the product for monitoring storage declines. When applied over aquifers experiencing significant land use change or below-average precipitation, the approach could monitor groundwater storage changes, even with limited *in situ* observations. The adaptable code is available for application in other study areas.

1. Introduction

A combination of mitigation and adaptation measures are essential to overcome the increasing pressure on global water resources

* Corresponding author.
E-mail address: cindy.viviers@tuks.co.za (C. Viviers).
[1] 0000–0002-7064–0818
[2] 0000–0001-8656–623X
[3] 0000–0002-6807–1353

https://doi.org/10.1016/j.ejrh.2024.101879
Received 21 February 2024; Received in revised form 17 June 2024; Accepted 18 June 2024
Available online 21 June 2024

amidst changing climate conditions (Sen, 2015; Sadath et al., 2023). Decision making for effective and sustainable groundwater resource management necessitates continuous, accurate and timely information of aquifer conditions (De Bruin et al., 2023). Groundwater level measurements are the primary information for evaluating hydrogeologic stresses acting on aquifers (Kenda et al., 2018). In places like South Africa (RSA), the distribution of hydrogeological monitoring stations is, however, inadequate or has decreased over the years, and where monitoring stations with publicly accessible data are active, the data storage infrastructure and formats are not standardised, obstructing data retrieval, sharing and integration into resource management (Gaffoor et al., 2020). The scarcity of reliable data at adequate spatial and temporal resolutions has prompted research into the viability of remotely sensed data as a potential alternative when high quality *in situ* data is unavailable (Milewski et al., 2019; Joseph et al., 2020).

The Gravity Recovery And Climate Experiment (GRACE) mission presented the first opportunity to directly measure water storage changes from space (https://grace.jpl.nasa.gov/applications /groundwater/ 2015). The distance between the twin satellites is measured meticulously, and fluctuations are attributed to the variations in the Earth's gravitational field, specifically reflecting mass redistribution in the hydrosphere (Swenson and Wahr, 2002). When the influence of mass transports from the ocean, atmosphere and Earth's interior are excluded, the temporal gravity field variations over land are primarily ascribed to Terrestrial Water Storage (TWS) change (Feng et al., 2013; Yan et al., 2022). Terrestrial water storage consists of all water on the land surface and subsurface combined (Yeh et al., 2006). To isolate a single component from the TWS, such as groundwater storage (GWS), the other estimated or measured components are subtracted from the total TWS (Feng et al., 2013).

Multiple studies have relied on the 0.25° Global Land Data Assimilation System (GLDAS) products to isolate the groundwater component from TWS (Alghafli et al., 2023; Strassberg et al., 2007; Feng et al., 2013; Liesch and Ohmer, 2016; Gaffoor et al., 2022; Ramjeawon et al., 2022). In early 2020, the GLDAS Version 2.2 (GLDAS-2.2) data products, assimilating GRACE data from the Centre for Space Research (CSR) into the Catchment Land Surface Model (CLSM) within the NASA Land Information System (LIS), were released. The method involves incorporating GRACE TWS observations into the model driven by meteorological data using a Kalman smoother approach to update and enhance the accuracy of forecasted model states (Li et al., 2019; Rui et al., 2022). Li et al. (2019) assessed how effectively GRACE Data Assimilation (GRACE-DA) enhances groundwater simulation across different regions worldwide. Of the African regions analysed in greater depth, Uganda serves as a proximate case study as the authors do not address RSA specifically. For Uganda, the authors found that GRACE-DA effectively reduced the dynamic range of CLSM-simulated GWS and improved interannual variability. This resulted in notable root mean square error (RMSE) and correlation improvements when compared to *in situ* observations, affirming that GRACE-DA significantly improved the accuracy of the GWS product, particularly in areas with substantial recharge. Overall, on a global scale, Li et al. (2019) observed that GRACE-DA improved simulation of GWS in GLDAS based on data from nearly 4 000 boreholes. Nevertheless, to be useful for local scale applications, coarse products often require downscaling (Gemitzi et al., 2021).

The primary objective of downscaling is to enhance the spatial resolution of a coarse dataset by integrating high-resolution information obtained from other sources. This can be achieved using either a dynamical or a statistical approach. Dynamical downscaling relies on assimilating boundary conditions from regional or global models and combining data from multiple sources to construct a process-based physical model at higher grid resolutions. Statistical downscaling is the process of analysing and establishing the empirical relationship between the coarse-resolution, regional variables and the corresponding more detailed, fine-resolution, local variables observed simultaneously in historical data. High-resolution, monthly time-series GWS estimates comparable to borehole observations could have significant benefits for groundwater resource assessments and management in RSA.

Statistical methods have been applied extensively in previous studies. For example, using the partial least squares regression statistical method and assimilating 0.5° water storage datasets from the WaterGAP hydrology model (WGHM) with precipitation, ET and runoff from other models, Vishwakarma et al. (2021) refined the GRACE TWS resolution from 3° to a 0.5°. The study demonstrated that the WGHM accurately redistributed water mass spatially while preserving mass conservation principles and signal amplitude. Yin et al. (2018) presented the correlative statistical downscaling relation method to downscale GRACE GWS anomalies (GWSA) from 110 to 2 km using only high-resolution Moderate Resolution Imaging Spectroradiometer (MODIS) ET data. The authors suggested the downscaling method may be applied for local water resource planning in areas where there is a strong relationship between GRACE TWS and ET. Given the importance of precipitation in TWS changes, Gemitzi et al. (2021) applied a spatial statistical downscaling method to downscale GRACE TWS from 1.0° to 0.1° relying solely on the Integrated Multi-satellite Retrievals for Global Precipitation Measurement precipitation dataset. The study, which considered temporal lags between precipitation and TWSA, found that the downscaled data closely matched independently modelled TWSA from 2005 to 2015, exhibiting strong performance across all evaluation metrics.

Several studies have applied machine learning (ML) algorithms to downscale GRACE data. Rahaman et al. (2019) and Ali et al. (2021) developed random forest (RF) models with multiple hydrological input variables [precipitation, evapotranspiration (ET), temperature, soil moisture storage, topography, surface runoff, plant canopy water storage and others] to downscale GRACE GWSA from 1° to 0.25°. Sabzehee et al. (2023) applied a RF model to forecast GRACE-derived GWSA and enhance the spatial resolution from 0.25° to 0.1° resolution, using precipitation, ET, land surface temperature (LST) and normalised difference vegetation index (NDVI) as predictors. The respective studies concluded that the RF models effectively increased the resolution of GRACE data and generated estimates that accurately capture groundwater level storage anomalies. None of these studies, however, investigated how incorporating temporal lags in the training process could minimise residuals.

Gaffoor et al. (2022) included local groundwater data, hydroclimatic parameters, and land-surface characteristics to train Gradient Boosting Decision Tree (GBDT) models. These models predicted groundwater level changes at a 10 km resolution for the karstic aquifers of the Ramotswa/Northwest/Gauteng Dolomites region, which encloses the Steenkoppies Dolomitic Compartment (SDC) included in this investigation. To assess the impact of hydroclimatic variables over different timeframes, the authors incorporated

arbitrary 30, 60 and 90-day increments as well as 30–60, 60–90, and 30–90 days intervals. Although the study did not specify the optimal temporal lag, it highlighted the importance of a 30-day gap for LST and GRACE-derived GWSA for model predictions.

Typically, studies use a variety of input variables to downscale GWS. A few reported studies relied solely on either precipitation or ET. This study hypothesised that GLDAS-2.2 GWSA can be downscaled to a 0.05° resolution using only two freely available, remotely sensed data products namely Climate Hazards Group InfraRed Precipitation with Station (CHIRPS) rainfall to capture recharge processes, and MODIS actual evapotranspiration (ET_a) to reflect discharge processes. The impact of accounting for temporal lags between variables on minimising residuals is often overlooked, especially in downscaling studies that apply residual correction. Using the Steenkoppies Catchment, RSA, this study further investigated the impact of incorporating temporal lags to reduce the adjustments (residuals) required for the high-resolution predictions. Additionally, most studies use an average specific yield (S_y) value for all aquifers across the entire study area when comparing the downscaled product to *in situ* groundwater levels. This study took a novel approach to optimising the S_y value per aquifer type. This highlighted the impact of groundwater level behaviour, characteristic to different aquifer types, on the downscaled product accuracy assessment. The modified approach offers valuable insights that should be considered when downscaled GWSA data are compared to *in situ* observations going forward. Effective statistical downscaling of GRACE-DA GWS can offer an innovative solution for understanding aquifer conditions when spatial or temporal data distribution is insufficient. Therefore, the analysis was done within the Google Earth Engine (GEE) environment for which the adaptable code is accessible for use in other study areas.

2. Materials and methods

2.1. Study area

The SDC is situated approximately 75 km south-west from the RSA capital city, Pretoria, primarily within the boundaries of quaternary catchment A21F (Fig. 1). Intensive irrigated agriculture has more than doubled across the SDC in the last 20 years (Vahrmeijer et al., 2013). The dominant crops cultivated throughout the year under pivot or sprinkler irrigation across the SDC are beetroot (*Beta vulgaris*), carrots (*Daucus carota*), lettuce (*Lactuca sativa*), cabbage and broccoli (*Brassica oleracea*), as well as maize (*Zea*

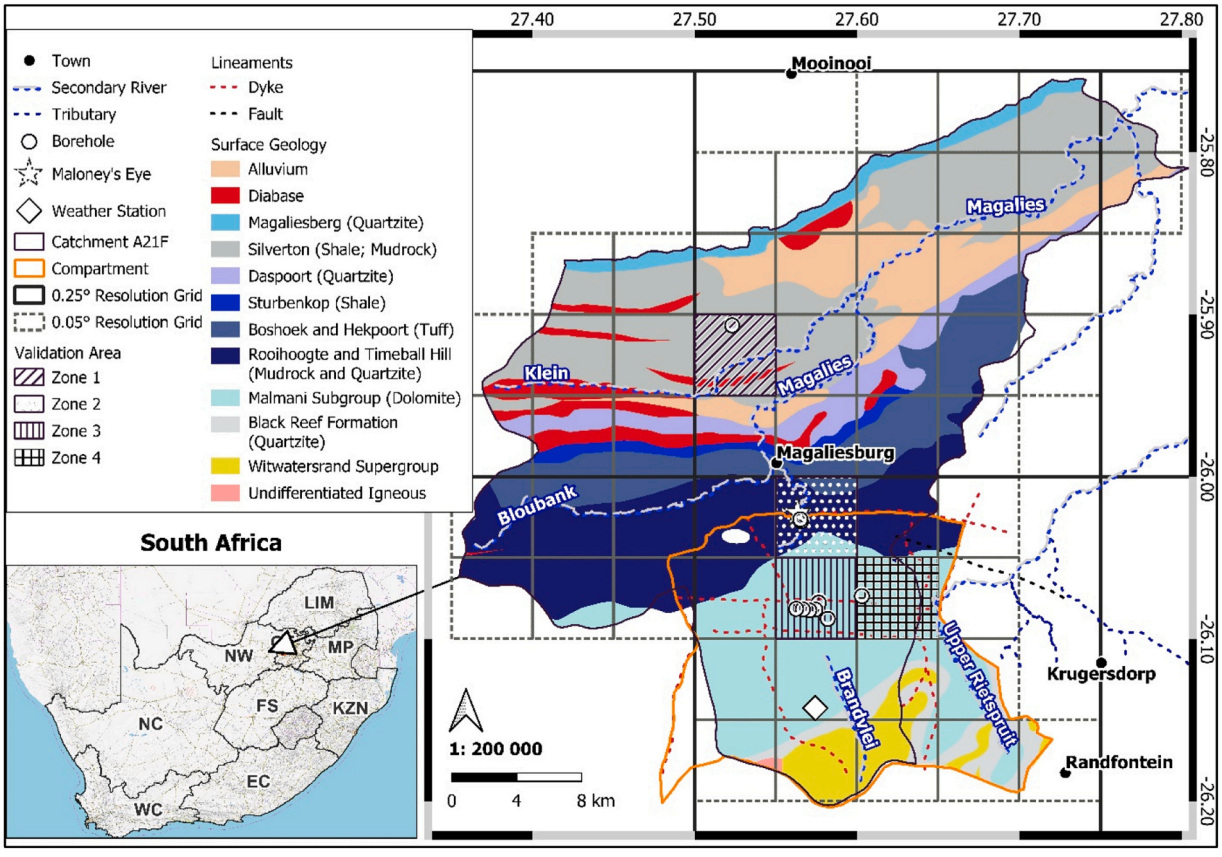

Fig. 1. Location and surface geology of the Steenkoppies Catchment (A21F) and Steenkoppies Dolomite Compartment, as well as the distribution of the downscaling validation *in situ* data in relation to the 0.25° Global Land Data Assimilation System (GLDAS)-2.2 Groundwater Storage (GWS) and the 0.05° downscale target resolution.

mays) in the summer and wheat (*Triticum aestivum*) in the winter (Le Roux et al., 2016). With an estimated surface area of 213 km^2, the SDC is a highly valuable groundwater resource for RSA, in terms of economic significance as well as employment (Holland and Wiegmans, 2009; Wiegmans et al., 2013). Since the spring flow decreased to 5.49 Mm^3a^{-1} in 2008, significantly lower than the long-term average flow of 14.38 Mm^3a^{-1} (Meyer, 2014), there has been an ongoing debate on whether decrease in GWS in the SDC is due to excessive groundwater abstraction or reduced precipitation (Holland and Wiegmans, 2009).

Based on the monthly data from the local automatic weather station (AWS) [Deodar (30619), −26.1427°S; 27.5743°E] (Fig. 1), with data from 2004 to 2021, the average temperatures range from a minimum of 15.9°C up to a maximum of 27°C in the summer, and the average winter temperatures range from a minimum of 2.2°C up to a maximum of 18.5°C. Based on CHIRPS data spanning from 1999 to 2021, the mean annual precipitation (MAP) across the A21F quaternary catchment calculated to 677 mm^1yr^{-1}, of which roughly 80 % occurs between November and March.

2.2. Geology and hydrogeology

The regional geology is primarily made up of the Transvaal Sequence, which includes a major karst aquifer formed within the dolomite rich Malmani Subgroup, along with the sequential intergranular and/or fractured aquifer formed in the eight Pretoria Group formations, namely the Rooihoogte Formation to the Magaliesberg Formation. The Pretoria Group formations comprise of alternating layers of mudrock and quarzitic sandstone units (Keyser, 1986; Eriksson et al., 2009; Moore et al., 2001). The region has been significantly deformed by post-Transvaal diabase and large-scale tectonic events.

The absence of surface water across the SDC suggests extensive recharge, where the surface water that would typically flow across the landscape is intercepted and infiltrates the dolomite aquifer characterised by numerous sinkholes (Wiegmans et al., 2013). Depending on specific geological conditions, the dividing dykes can form isolated hydrological compartments with a flat groundwater level table and relatively uniform groundwater conditions, with less significant abstraction and flow impact between compartments in comparison to within a compartment. Dolomite compartment boundaries are typically associated with spring lines and seepages as the groundwater is forced to the surface (Holland and Wiegmans, 2009; Bredenkamp et al., 1986; Kuhn, 1986).

Analysis of the depth to groundwater level data since 2000 indicate significantly deeper groundwater levels in the karst aquifer (averaging around 64 m) compared to the northern intergranular and/or fractured aquifers, where the average depth is approximately 9 m.

2.3. Data and pre-processing

2.3.1. GLDAS-2.2 groundwater storage data

Vishwakarma et al. (2018) determined that a minimum catchment size of 63 000 km^2 is observable using filtered GRACE fields and more advanced techniques are necessary to detect mass variations at finer resolutions. The CSR mascon solution relies solely on GRACE data, independent from TWS and external models. The solutions are computed using a custom hexagonal grid (approximately 120 km or 1° at the equator), which offers improved spatial resolution over traditional spherical harmonics (Chen et al., 2017; Save et al., 2016).

Dynamic downscaling assimilates coarse-resolution data to develop a model applicable to finer resolution data (Rahaman et al., 2019). The GLDAS-2.2 is specifically engineered to integrate various observational data products to enhance its land surface models. Data Assimilation has been applied to combine remotely sensed GRACE TWS data with the fine 2.5 km grid CLSM in LIS Version 7 estimates driven by meteorological inputs, land cover, soil, topography, and other model-specific parameters to estimate fluctuations in water content at a 0.25° spatial resolution.

The GLDAS-2.2 product provides disaggregated and continuous water storage estimates, which include GWS computed as TWS minus the root zone soil moisture to a depth of 1 m, the snow water equivalent, and any canopy interception (Rui et al., 2022). Before assimilating the GRACE data, provided as anomalies in mm, the 2003–2015 temporal mean of the simulated TWS open-loop run (averaged to each 0.5° GRACE grid) was added to the GRACE TWS measurements. This was done to make the GRACE TWS comparable to the GLDAS-2.2 TWS for assimilation (Li et al., 2019). Hence to convert the GLDAS-2.2 data back to anomalies comparable to GRACE measurements, the 2003–2015 temporal mean must be subtracted. The GLDAS-2.2 (NASA_GLDAS_V022_CLSM_G025_DA1D) data extending from March 2003 to December 2021 was accessed and processed through GEE.

2.3.2. Climate hazards group InfraRed precipitation with station (CHIRPS) precipitation data

The satellite-gauge gridded precipitation product, CHIRPS, extending from 50°S to 50°N (and all longitudes) and dating from 1981 to near-present, is obtained from an algorithm combining precipitation datasets from different sources into a single product (Funk et al., 2015). The 0.05° (5566 m) CHIRPS precipitation (UCSB-CHG_CHIRPS_DAILY) product, released at a daily temporal resolution, was used to calculate monthly precipitation, and reprojected to align with the GWS.

Historically, remotely sensed data has been criticised for its perceived lack of accuracy, but remarkable advancements in accuracy have been made over the past three decades (Karimi and Bastiaanssen, 2015). Despite these improvements, it is important to maintain a critical perspective. To evaluate the consistency between monthly *in situ* observations and the CHIRPS product, the data from the Deodar AWS was compared against both the pixel in which it was located and the pixel immediately south from the AWS, as the station was located near the border to this adjacent pixel (see Fig. 1).

Because the GRACE data are provided as anomalies, specifically deviations relative to a 2004–2009 baseline temporal average, and the 2003–2015 GLDAS-2.2 temporal mean was subtracted to make the GLDAS-2.2 measurements comparable to GRACE, the monthly

CHIRPS estimates were standardised to anomalies by computing the 2004–2009 mean and then subtracting that mean.

2.3.3. Moderate resolution imaging spectroradiometer (MODIS) evapotranspiration

The MODIS ET_a data product is estimated using a modified (Mu et al., 2011) Penman-Monteith equation (Monteith, 1965) that improves the accuracy and spatial resolution of ET_a estimates by integrating daily meteorological reanalysis data, as well as eight-day MODIS remotely sensed data products that capture the effect of land cover and vegetation dynamics on ET_a. The MOD16 ET_a is the sum of canopy transpiration, soil evaporation and interception evaporation (Mu et al., 2007 and Mu et al., 2011).

Within GEE, the 0.005° eight-day composite ET_a (MODIS_006_MOD16A2) (Running et al., 2021) data were first filtered for a 'clear' cloud state and a quality control confidence state of 'best result possible with no saturation'. Following quality control, the monthly mean ET_a was quantified, reprojected to match the GWSA, and resampled to the spatial resolution of CHIRPS. To standardise the ET_a

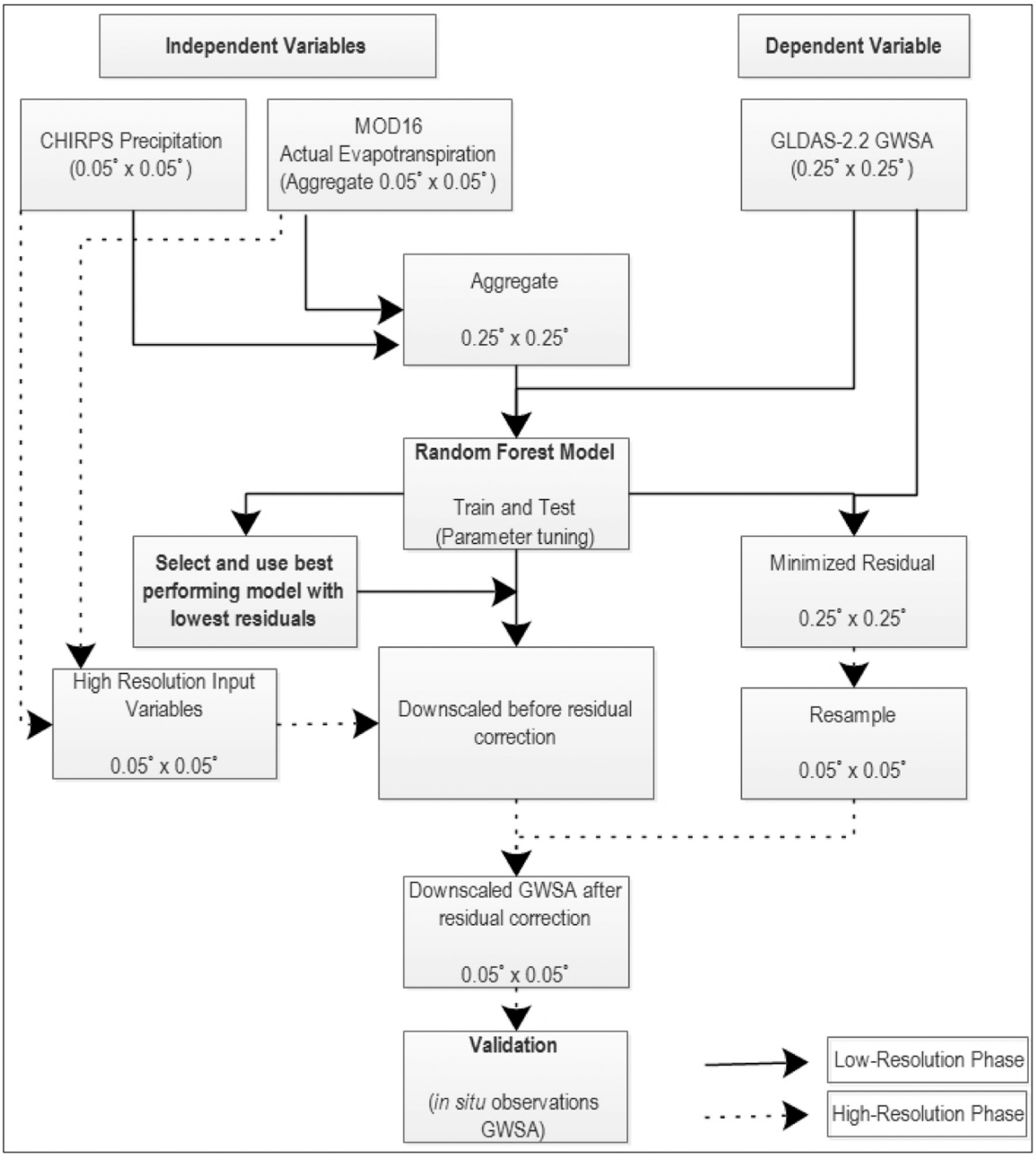

Fig. 2. Flowchart of the downscaling model design in this study (CHIRPS - Climate Hazards Group InfraRed Precipitation with Station, MODIS - Moderate Resolution Imaging Spectroradiometer, GLDAS-2.2 Global Land Data Assimilation System (GLDAS) Version 2.2, GWSA - Groundwater Storage Anomaly).

data to anomalies comparable to the GWSA, the 2004–2009 temporal mean was calculated and then subtracted.

2.4. Input variable selection and correlation analysis

High precipitation coupled with lower ET_a generally results in increased water availability for infiltration and percolation into the groundwater (Cao et al., 2013; Moiwo et al., 2011). In this study, precipitation was selected because aquifer recharge is primarily from precipitation, and the relationship with groundwater level fluctuations and discharge from the Maloney's Eye spring is well documented (Wiegmans et al., 2013; Vahrmeijer et al., 2013). Actual evapotranspiration was selected because it is considered a key process within the hydrological cycle which reflects varying factors such as weather conditions, landscape and topography, vegetation and land use cover, and soil properties (Mu et al., 2007).

The impact of precipitation and ET_a is not immediately reflected in GWS and lags due to factors such as the unsaturated zone thickness, and the transmissivity and storage characteristics of the underlying lithology (Kotchoni et al., 2019). To evaluate whether precipitation and ET_a can be applied as independent variables for downscaling, the temporal correlation coefficient (r) was quantified per 0.05° pixel using cross-correlation. The r was calculated by shifting the precipitation and the ET_a values with a range of time lags spanning from one to twelve months prior to calculating the r against the reference GWS at every lag. The lag time periods that produced the highest aggregated mean r across the study area was selected and integrated into the downscaling design for Model 2.

2.5. Random forest and downscaling model design

2.5.1. Random forest model

The RF supervised learning algorithm is a non-linear statistical learning method that deals with multiple, uncorrelated decision tree combinations to overcome the bias and overfitting problem associated with single decision trees (Shelestov et al., 2017). The average prediction for the ensemble of trees is the output. The effectiveness of the RF algorithm lies in its principle of leveraging the 'collective wisdom of a committee of predictions', which is more accurate than any individual tree (Yiu, 2019; Srivastava et al., 2023).

Each tree is trained on a different random subset (bag fraction) of the same training set. The bag fraction implies the percentage of total training data randomly selected with replacement (bootstrapping) for training each tree. The remaining training data makes up the 'out-of-bag' sample, which acts as a mini test within the model to evaluate the performance of the tree unbiasedly (Brownlee, 2020). A decision tree is trained by branching out into increasingly homogeneous subsets from the root node until reaching 'leaves' that are nodes without further sub-division. The root node begins with the complete training data subset, repeatedly splitting the data according to the independent, predictor variables. At every node, the algorithm calculates the prediction improvement for each variable's split point, choosing the split that results in the highest improvement. To evaluate the 'improvement' made per threshold (node condition), the model calculates the sum of the squared residuals between the node and its child nodes after the split (Hoare, 2023).

Studies have shown that RF models outperform support vector regression (SVR), artificial neural network (ANN) and multivariate linear regression (MLR) ML models in downscaling GRACE data to a higher spatial resolution (Chen et al., 2019, Ali et al., 2021 and Sabzehee et al., 2023). Hence, the RF model was considered suitable for this downscaling GLDAS-2.2 GWSA application.

2.5.2. Random forest downscaling model design

For model training and performance assessment, the projections and scale of the precipitation and ET_a data were aligned and regridded (using nearest neighbour resampling) to match the 0.25° GWSA. Two respective RF models were trained using data spanning from January 2003 to December 2016 (thirteen years or 72 % of the available time-series). The respective models differed only in one aspect of model design (Fig. 2) namely 'Model 1' had no temporal lag incorporated for the input variables, versus for 'Model 2' precipitation was adjusted by a three-month lag and ET_a by a two-month lag for optimised r with GWS, as described in Section 2.4.

To evaluate the prediction performance of the trained models, the respective RF models were applied to predict 0.25° GWSA for the separate testing dataset extending from January 2017 to December 2021 (five years or 28 %). Several combinations of the number of trees (ranging from 10 to 150 in increments of 10) and bag fraction (varying from 0.1 to 0.5 in increments of 0.1) were evaluated to determine the optimal setting for minimising RMSE. These evaluations were done by comparing the new 0.25° predicted GWSA against the original 0.25° GWSA data (before any residual correction). The combination that resulted in the lowest RMSE involved 150 trees for Model 1 and 110 trees for Model 2, both with a bag fraction of 0.5. The remaining model arguments, including variables per split, the minimum number of samples required to form a leaf node, the maximum depth of trees, and seed, were left at their default settings in GEE. There is not an option to explicitly select the loss function in GEE, but the default loss function for model training is Mean Squared Error (MSE).

The best performing RF model was then applied to predict coarse-resolution GWSA for the complete timeframe using the 0.25° resolution precipitation and ET_a data as input variables. Pixel-wise residuals were computed by subtracting the new predicted GWSA from the original GWSA, essentially calculating the low-resolution model error. To accurately adjust for errors visible from the low-resolution model, when predicting high-resolution GWSA, these residuals were disaggregated to the 0.05° scale using nearest neighbour resampling.

Subsequent to model training and residual computation, the best performing RF model was applied to predict high-resolution GWSA estimates using the 0.05° high-resolution input variables. As per the established approach (Chen et al., 2019; 2023), the disaggregated residuals were then added to the new high-resolution GWSA estimates (residual correction) to generate monthly GWSA estimates at a finer resolution. For each respective zone, the 0.05° downscaled GWSAs were then evaluated against the *in situ*

groundwater level storage anomalies. When adapting the script for new areas of interest, the comparison of model output to available *in situ* data should not be neglected.

2.6. Data validation and error analysis

To conduct a quantitative evaluation of the time-series datasets, the metrics used include the r (Eq. 1), RMSE (Eq. 2) and mean absolute error (MAE) (Eq. 3). The r was calculated by determining the covariance and dividing the covariance by the product of the variables' standard deviations. The r can vary between −1 and 1, where 1 signifies a model that perfectly captures the synchronised rise and fall of the two variables. The RMSE and MAE metrics gauge how close the model predictions are to the actual values. A value near 0 indicates a highly accurate model.

$$r = \frac{\sum_{i=1}^{n}(X_i - \overline{X})(Y_i - \overline{Y})}{\sqrt{\sum_{i=1}^{n}(X_i - \overline{X})^2}\sqrt{\sum_{i=1}^{n}(Y_i - \overline{Y})^2}} \tag{1}$$

$$RMSE = \sqrt{\frac{\sum_{i=1}^{n}(X_i - Y_i)^2}{n}} \tag{2}$$

$$MAE = \frac{1}{n} * \left(\sum_{i=1}^{n}|Y_i - X_i|\right) \tag{3}$$

Where $X_i and \quad Y_i$ indicate the input variable and the predicted variable, respectively, and $\overline{X} and \overline{Y}$ indicate the respective means of the dataset with 'n' representing the sample count.

2.7. In situ groundwater level monitoring data for validation

Groundwater level monitoring data suitable for comparison with remotely sensed GWSA estimates should be sensitive to atmospheric conditions, accurately reflect seasonal fluctuations, and the record should span across at least five years to ensure strong statistical analyses (Rodell et al., 2007, Li et al., 2019). Groundwater level monitoring data across the study area were sourced from the Hydstra Data Management platform (https://www.dws.gov.za/Groundwater/data.aspx, received March 2022), which includes data from the Department of Water and Sanitation (DWS) Groundwater Monitoring Network.

During data pre-processing, the records received were limited to within the specified study timeframe of 2002–2021, resulting in approximately 1 750 observations distributed over thirteen boreholes. Two boreholes were excluded for having ten or less observations over the 2004–2009 timeframe. Outliers were identified using the interquartile range method (IQR) and visualisation, after which outliers were either retained or removed. The result was 1 480 observations distributed over 11 boreholes (Fig. 1).

To quantitatively compare *in situ* measurements to downscaled GWSA, the temporal 2004–2009 groundwater level mean ($GWL_{2004-2009mean}$), recorded as depth to groundwater level (in meters) from the topographic surface per monitoring borehole, was first calculated before being subtracted from the respective measurements (GWL_i) to create a time-series anomaly of above (positive) or below (negative) mean depth to groundwater level (Eq. 4). The respective groundwater level anomaly measurements ($GWL_{Anomaly}$) were then converted from m to mm (unit comparable to GLDAS GWSA) and multiplied by the aquifer specific yield (S_y) to change the time-series groundwater level anomalies to storage anomalies ($GWS_{Anomaly}$) (Eq. 5).

$$GWL_{Anomaly} = GWL_i - \quad GWL_{2004-2009mean} \tag{4}$$

$$GWS_{Anomaly} = (GWL_{Anomaly} \quad \times \quad 1000) \quad \times \quad S_y \tag{5}$$

Using a 0.05° resolution grid, the observation boreholes were distributed over four distinct verification zones as visualised in Fig. 1. Proceeding from north to south, Zone 1 corresponds with the intergranular and fractured Pretoria Group Aquifer and Zone 2 with two boreholes situated near Maloney's Eye. Zone 3 and Zone 4, which encompassed a cluster of seven boreholes and a solitary borehole, respectively, were positioned over the SDC.

In contrast to the r metric, both RMSE and MAE are considerably dependent on the S_y value. To ensure a representative and accurate comparison between the downscaled GWSA estimates and the *in situ* observation derived GWSA, the authors methodically adjusted the S_y values at intervals of 0.01, spanning from 0.01 to 0.1. The optimal S_y value which resulted in the lowest RMSE and MAE across the SDC and the intergranular and/or fractured aquifer, respectively, was selected.

3. Results and discussions

3.1. Validation of CHIRPS

It is important to recognise the inherent errors when validating remotely sensed data against point observations. These discrepancies are primarily ascribed to the partial coverage of the remote sensing area by the measurement footprint (Twine et al., 2000, Allen et al., 2011). The Deodar AWS data were evaluated against both the intersected CHIRPS pixel and the pixel immediately adjacent from the AWS at a monthly, seasonal, and annual temporal resolution (Table 1). The remotely sensed CHIRPS product offers a good alternative monthly rainfall data source where the *r* to rainfall station data is good (Du Plessis and Kibii, 2021).

At an annual temporal resolution, the 2004–2021 MAP calculated to 637 mm^1yr^{-1} for the AWS compared to 648 mm^1yr^{-1} and 667 mm^1yr^{-1} for the intersected and AWS adjacent CHIRPS pixel, for the same period. The seasonal analysis revealed that during summer (Su – December, January and February) and winter (W – June, July and August), the *r* were lower compared to spring (Sp – September, October and November) and autumn (A – March, April and May). These findings are consistent with the research by Du Plessis and Kibii (2021), which evaluated CHIRPS against 46 evenly distributed rainfall stations across RSA. Du Plessis and Kibii (2021) also found that CHIRPS demonstrated optimal accuracy before (spring) and after (autumn) the summer rainfall seasonal.

Du Plessis and Kibii (2021) observed a tendency for CHIRPS to overestimate low rainfall and underestimate high rainfall events. In Fig. 3, a positive deviation from the AWS measurement indicated CHIRPS overestimation whereas a negative difference indicated an underestimation of the monthly CHIRPS estimate compared to the *in situ* measurement. The analysis confirmed a significant *r* at a monthly temporal resolution, confirming that CHIRPS estimates capture the local, temporal variations in precipitation well. Additionally, it was concluded that the intersected pixel represented the AWS more accurately than the adjacent pixel directly south from it.

3.2. Temporal correlation analyses

The variation in the aggregated mean monthly precipitation (CHIRPS), MODIS ET_a and GWSA across quaternary catchment A21F from 2017 to 2021 is displayed in Fig. 4a. The highest *r* was achieved when accounting for a three-month precipitation lag (0.61) and a two-month ET_a lag (0.65) until the response in GWSA was reflected. Using a harmonic analysis, the average seasonal variability of precipitation, ET_a and GWSA were characterised (Fig. 4b), and concluded that the monthly precipitation peak in January, as is anticipated for a summer rainfall region, aligned with ET_a peaking in January and February. The seasonal GWSA trends indicated aquifer recovery and an increase in GWS starting from the lowest point in October reaching a maximum peak in April. However, subsequent to this peak, the aquifer storage decreased as outflow surpassed inflow when crop irrigation intensified during the dry autumn and winter months (May to August).

The spatial distribution of the GWSA and lagged precipitation *r* ranged from 0.56 to 0.62, as illustrated in Fig. 5a, whereas the *r* between GWSA and lagged ET_a varied between 0.58 and 0.7 (Fig. 5b). Statistical analysis confirmed the significance of these correlations at the 1 % level, with pixel-wise p-values well below 0.01. This suggests that the observed correlation is unlikely to have occurred by chance. The *r* between the three-month lagged precipitation and two-month lagged ET_a ranged from 0.83 to 0.88 across the study area, with an average *r* of 0.86.

An insignificant *r* between the GWSA and precipitation would indicate that GWS does not respond and recover following precipitation events, and that the aquifer is being unsustainably exploited, or that land use, such as irrigation, is resulting in GWS recovery in the absence of a precipitation event. A stronger *r* in some parts can be ascribed to the spatial heterogeneity of factors that affect groundwater recharge (Rukundo and Doğan, 2019). The *r* is somewhat stronger across the SDC distinguished by numerous sinkholes and a flat undulating plain, and weaker towards the western section of the study area characterised by steeper slopes.

Table 1
Pairwise metric comparison between *in situ* and remotely sensed precipitation estimates.

	Intersected pixel			Pixel immediately adjacent to the AWS		
	Annual	**Seasonal**	**Monthly**	**Annual**	**Seasonal**	**Monthly**
r	0.47	Su – 0.44 A – 0.87 W – 0.56 Sp – 0.74	0.82	0.48	Su – 0.45 A– 0.88 W - 0.54 Sp – 0.73	0.82
RMSE (mm)	124.4	Su – 48 A - 26 W - 10 Sp - 30	31.9	127.3	Su – 50 A - 25 W - 10 Sp - 31	32.3
MAE (mm)	94.1	Su – 36 A- 19 W - 6 Sp - 20	20.3	90.5	Su – 38 A - 19 W - 6 Sp - 20	21

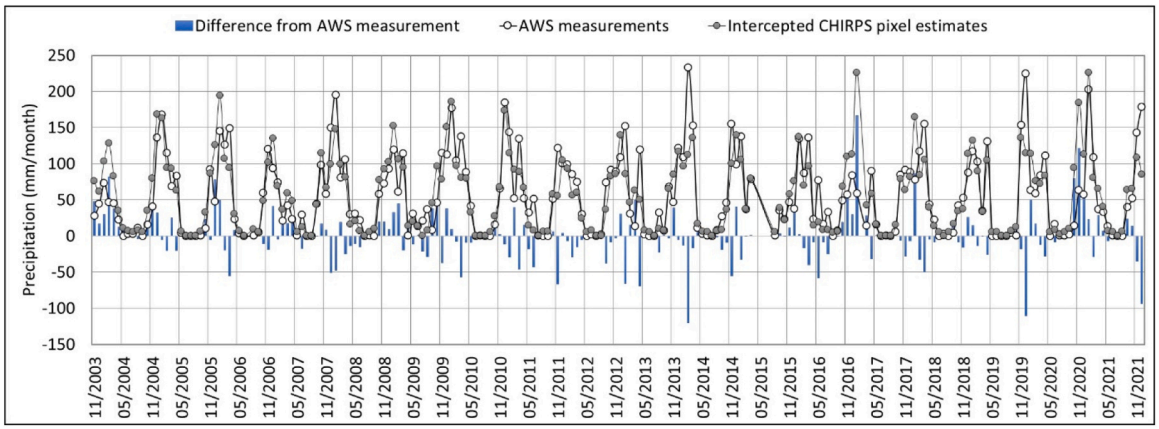

Fig. 3. Monthly Deodar automatic weather station (AWS) measurements in comparison to the intercepted Climate Hazards Group InfraRed Precipitation with Station (CHIRPS) data estimates, and the difference between CHIRPS and measured *in situ* data.

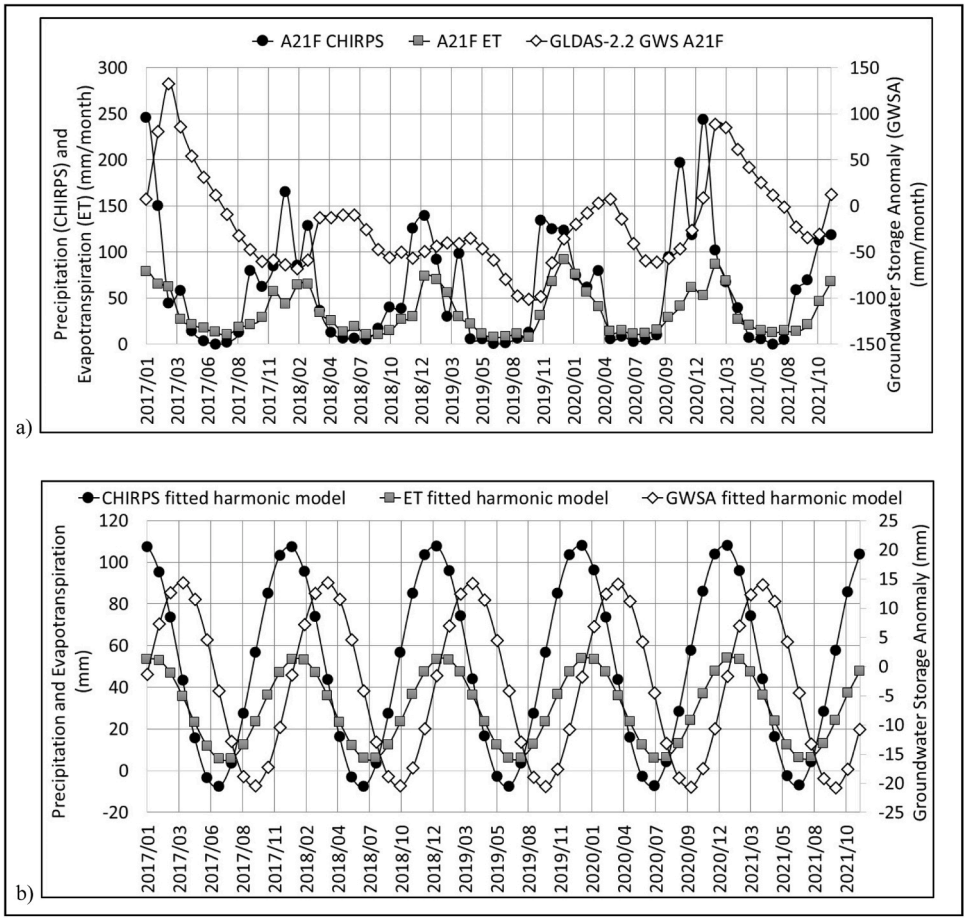

Fig. 4. Temporal variation of monthly Climate Hazards Group InfraRed Precipitation With Station Data (CHIRPS) precipitation, Moderate Resolution Imaging Spectroradiometer (MODIS) actual evapotranspiration (ET_a) and Global Land Data Assimilation System (GLDAS-2.2) Groundwater Storage Anomaly (GWSA), using the spatially aggregated average across quaternary catchment A21F: (a) Time-series monthly changes and (b) fitted harmonic model to characterise seasonal variability.

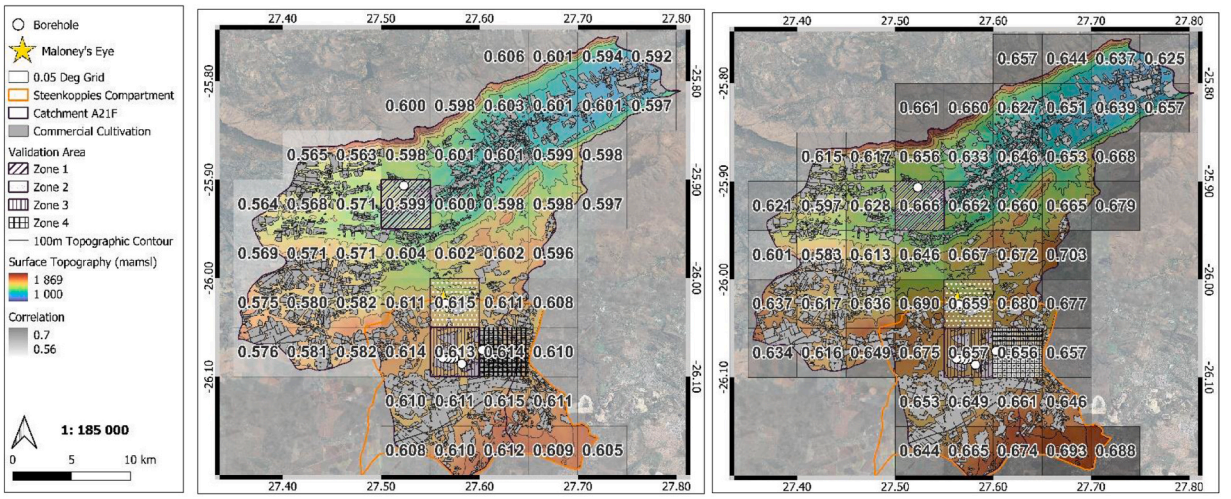

a) b)

Fig. 5. Spatial distribution of the temporal correlation between the Global Land Data Assimilation System (GLDAS-2.2) Groundwater Storage Anomaly (GWSA) to the a) three months lagged Climate Hazards Group InfraRed Precipitation With Station Data (CHIRPS) precipitation estimates and b) two months lagged Moderate Resolution Imaging Spectroradiometer (MODIS) evapotranspiration (ET_a) estimates at a monthly temporal and 0.05° spatial resolution. Commercial cultivation from (Crop Estimates Consortium (2021); Crop Estimates, 2021)

3.3. Random forest model performance analysis

Machine learning model performance metrics (Table 2) were computed by comparing the 0.25° predicted GWSA to the original GLDAS GWSA for the separate testing dataset before any residual correction, as illustrated in Fig. 6. The initial comparison demonstrates the inherent predictive capabilities of each model based on parameters and the training data (Jain et al., 2023). The model performance metrics demonstrated that Model 2 outperformed Model 1 as is evident from the higher *r*, combined with the lower RMSE and MAE values. Fig. 6 demonstrated that Model 2 had lower residuals and fewer outliers compared to Model 1.

Residual correction applied to the predictions addressed low-resolution model inaccuracies and corrected for these inaccuracies in the high-resolution product. Minimising residuals not only improved the accuracy of the low-resolution model but also reduced the adjustments to the high-resolution predictions, thereby enhancing the reliability and accuracy of the high-resolution estimates predicted.

3.4. Mass conservation

Downscaling aims to redistribute groundwater mass using additional, high-resolution information while upholding the principle of mass conservation. Vishwakarma et al. (2021) validated the efficiency of downscaled outputs by assessing mass conservation at catchment scale. To confirm mass conservation at catchment scale and the ability of the downscaled product to provide mass change estimates at higher spatial resolution, the authors compared the monthly total of the coarse-resolution GLDAS-2.2 GWSA across the catchment with the monthly total of the downscaled GWSA estimates (Fig. 7). The assessment yielded values of 0.98 for *r*, 330 mm for RMSE, and 265 mm for MAE.

GRACE data characteristically have a low-resolution with strong spatial correlation between neighbouring GRACE grids (Seyoum et al., 2019). The long-term standard deviation (2003–2021) GWSA before (Fig. 8a) and after (Fig. 8b) downscaling was compared to assess the similarity and whether the downscaled data preserves the spatial distribution of the original data. The similarity of the spatial distribution between the coarse and finer resolution datasets are apparent in Fig. 8. The greater range of downscaled GWSA values indicated that the high-resolution output effectively integrated the precipitation and ET_a input variables. It was therefore hypothesised that the downscaled product captured spatial differences and details, such as temperature, slope, and land cover represented by the ET_a variable, as well as recharge events linked to precipitation, to provide a more comprehensive reflection of

Table 2
Model performance metrics calculated for Models 1 and 2 before residual correction.

	Model 1	Model 2
r	0.35	0.6
RMSE (mm)	49	45
MAE (mm)	40	38

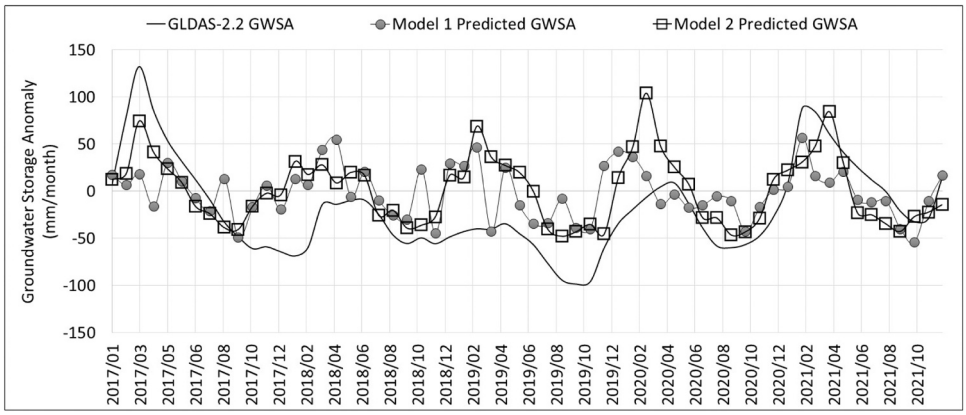

Fig. 6. Performance assessment of the respective machine learning models for predicting 0.25° Groundwater Storage Anomaly (GWSA) using Model 1 input variables without temporal lags, and Model 2 with input variables adjusted with the respective temporal lags.

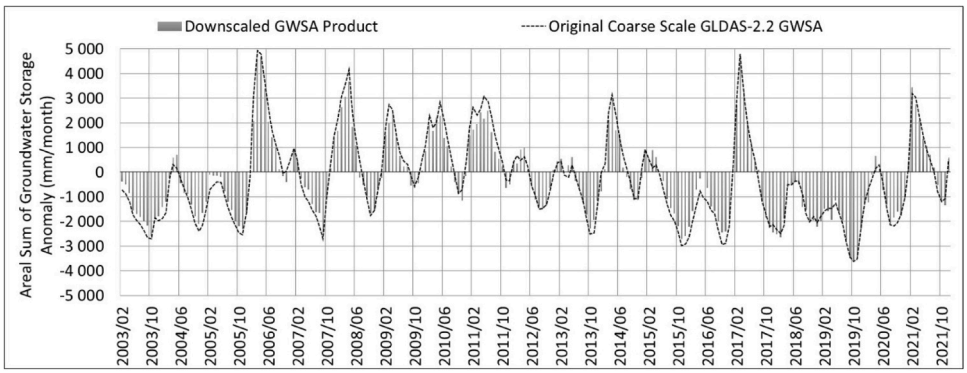

Fig. 7. Monthly sum of the groundwater storage anomalies (GWSA) across catchment A21F for the downscaled product and the original coarse-resolution Global Land Data Assimilation System Version 2.2 (GLDAS-2.2) product.

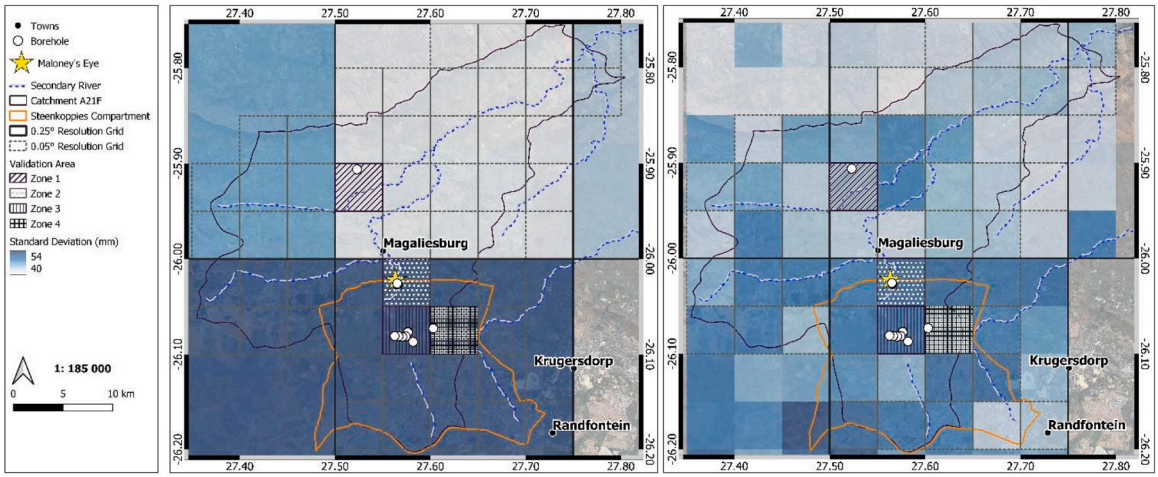

a) b)

Fig. 8. The geographic distribution of the Groundwater Storage Anomaly (GWSA) standard deviation (2003 – 2021) before (a) and after (b) downscaling.

groundwater dynamics.

3.5. Validation of downscaled GWSA data

The S_y values which resulted in the lowest RMSE and MAE (Table 3) were 0.02 across the intergranular and/or fractured aquifer and 0.04 for the karst aquifer boreholes. These S_y values correspond to the average S_y of 0.01 for the intergranular and/or fractured aquifer and the average of 0.035 for the dolomitic aquifer, which were used by Wiegmans et al. (2013) to calibrate their numerical model for the study area.

The validation results were achieved by comparing the downscaled GWSA to the *in situ* derived GWSA (Fig. 9). Apart from having the highest *r,* Zone 1 exhibited the lowest RMSE and MAE, in contrast to Zone 2 and Zone 3, which displayed higher RMSE and MAE values. The *r* for Zone 4 was comparable to that of Zone 2, and Zone 4 exhibited the lowest RMSE and MAE across the SDC. This is ascribed to the larger GWSA amplitudes, or seasonality, depicted in the *in situ* groundwater level data for Zone 1, but less so for Zones 2, 3 and 4. This phenomenon can be attributed to the characteristic groundwater level behaviour in karst aquifers and near springs which remain more stable due to the highly permeable nature of the aquifer, and the flow through the dolomitic subsurface into the less conductive shales and quartzites. Gaffoor et al. (2022) achieved a MAE of approximately 170 mm in predicting current groundwater level changes for the SDC by incorporating thirteen variables and pre-determined temporal lags into GBDT models. Using only two input variables adjusted with the optimal lag to GWSA resulted in an average MAE of 37 mm across the SDC in this study.

It is important to recognise that S_y varies horizontally and vertically within the same unconfined aquifer, and hence relying on a single value to characterise the entire aquifer simplifies a complex system (Chen et al. 2010). A higher S_y value of around 0.1 would be required for the *in situ* derived GWSA to reach the downscaled GWSA highs (shallower groundwater level) across the SDC, but this is not an aquifer representative average nor did 0.1 result in the lowest RMSE and MAE values. While high S_y values may be feasible in karst aquifers, they are likely not characteristic of the entire karst system but rather specific zones within the aquifer (Yu et al. 2022; Rose et al. 2018).

The downscaled data indicated that the groundwater levels decrease and then recover following precipitation events as observed with the *in situ* data. This demonstrated the potential of the downscaled product in monitoring whether the SDC is currently experiencing a decline in groundwater storage. If the downscaling was done over a period of consecutive years below average precipitation, or over other aquifers undergoing substantial land cover and water use changes, these trends could be detected in the downscaled GWS product, allowing site-specific interventions, even when few *in situ* borehole measurements are available. It would be recommended that the downscaled GWS estimates complement rather than replace *in situ* measurements.

When evaluating the downscaled GWSA, it is important to acknowledge known uncertainties. These uncertainties include the limited distribution of observed measurements and the challenges of directly validating high-resolution ET_a data against observed data. Additionally, local GWSA decreases unrelated to low precipitation and high ET_a, such as abstraction for domestic or industrial purposes, may not be fully accounted for by the downscaled product. These important aspects are recommended for future research.

4. Conclusions

The study presented a simple framework for downscaling GWSA from 0.25° to 0.05° in the GEE cloud computing platform using the RF ML algorithm and only precipitation and ET_a as input variables. The comparison between the coarse-resolution and downscaled GWSA estimates concluded that the downscaled estimates incorporated spatial precipitation and ET_a variations to reveal differences in recharge and discharge processes while adhering to the mass conservation principle. Accounting for the temporal lags between input variables improved the accuracy of the low-resolution model and reduced the residuals added to the high-resolution predictions.

The use of high spatial resolution, monthly time-series GWSA estimates can be applied to fill *in situ* groundwater data gaps (Sahour, 2020), develop an efficient validation network, and to enhance the determination of high-resolution hydrogeological parameters such as groundwater recharge. Since the accuracy assessment and application of the downscaled GWSA necessitates careful consideration of how groundwater levels respond in different aquifers, future work could include an even more refined downscaling outcome by applying an adaptive approach where a separate RF model is trained for each aquifer type, and where viable *in situ* observations are included as an input variable. The use of varying S_y values should also be considered. Nevertheless, this study demonstrated the practical application of using open-source remotely sensed products combined with ML to produce localised groundwater information to enhance groundwater management, particularly in regions with limited data availability. The code has been made freely available to all.

CRediT authorship contribution statement

Cindy Viviers: Writing – original draft, Visualization, Validation, Methodology, Formal analysis, Conceptualization. **Michael van der Laan:** Writing – review & editing, Validation, Supervision, Funding acquisition, Conceptualization. **Matthys Dippenaar:** Writing – review & editing, Supervision. **Zaheed Gaffoor:** Writing – review & editing, Validation, Methodology.

Declaration of Competing Interest

The authors declare the following financial interests/personal relationships which may be considered as potential competing

Table 3
Comparison metrics between the *in situ* groundwater level storage and the downscaled Groundwater Storage Anomaly (GWSA) for the respective zones.

	Zone 1	Zone 2	Zone 3	Zone 4
r	0.6	0.48	0.30	0.44
RMSE (mm)	40	50	49	42
MAE (mm)	31	41	39	36

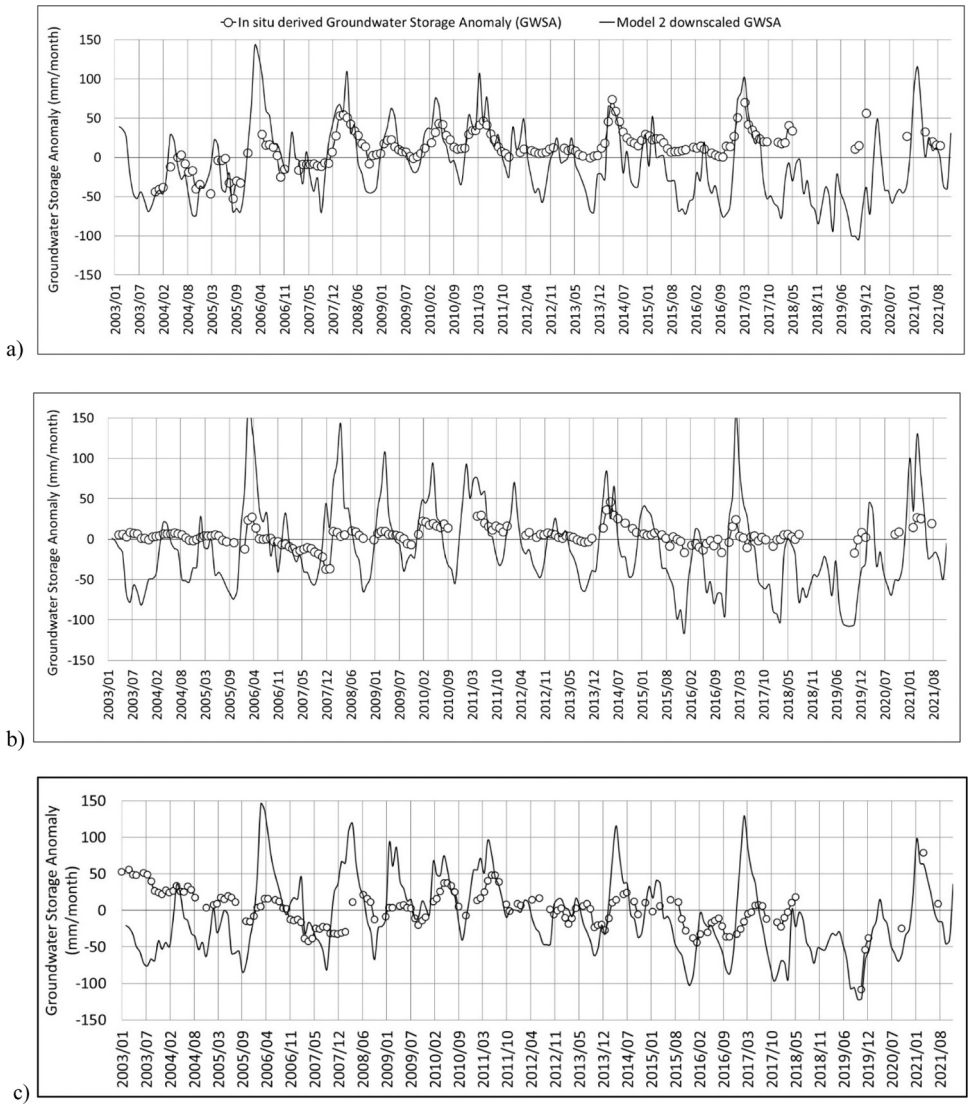

Fig. 9. Comparison between groundwater level storage and the downscaled Groundwater Storage Anomaly (GWSA) for Zone 1 (a), Zone 2 (b) and Zone 3 (c) (Zone 4 is not illustrated as it is visually not highly distinguishable from Zone 3).

interests: Cindy Viviers reports financial support was provided by Water Research Commission. If there are other authors, they declare that they have no known competing financial interests or personal relationships that could have appeared to influence the work reported in this paper.

Data availability

Code included - https://code.earthengine.google.com/9019a84556ec0cdf0337aae14dfde178

Acknowledgements

The authors would like to thank the Water Research Commission for the funding of project number C2020/2021–00440, as well as the Agricultural Research Council (ARC) for providing the AWS data for this study.

Appendix A. Supporting information

Supplementary data associated with this article can be found in the online version at doi:10.1016/j.ejrh.2024.101879.

References

Alghafli, K., Shi, X., Sloan, W., Shamsudduha, M., Tang, Q., Sefelnasr, A., Ebraheem, A.A., 2023. Groundwater recharge estimation using in-situ and GRACE observations in the eastern region of the United Arab Emirates. Sci. Total Environ. 867, 161489 https://doi.org/10.1016/j.scitotenv.2023.161489.

Ali, S., Liu, D., Fu, Q., Cheema, M.J.M., Pham, Q.B., Rahaman, M.M., Dang, T.D., Anh, D.T., 2021. Improving the resolution of GRACE data for spatio-temporal groundwater storage assessment. *Remote Sens.* 2021 13, 3513. https://doi.org/10.3390/rs13173513.

Allen, R.G., Pereira, L.S., Howell, T.A., Jensen, M.E., 2011. Evapotranspiration information reporting: I. Factors governing measurement accuracy. Agric. Water Manag. 98, 899–920. https://doi.org/10.1016/j.agwat.2010.12.015.

Bredenkamp D.B., Van der Westhuizen C., Wiegmanns F.E., Kuhn C.M. 1986. Groundwater supply potential of dolomite compartments west of Krugersdorp. Technical Report GH3440. Directorate Geohydrology. Department of Water Affairs and Forestry, Pretoria.

Brownlee L. 2020. Bagging and Random Forest Ensemble Algorithms for Machine Learning. Machine Learning Mastery.https://machinelearningmastery.com/bagging-and-random-forest-ensemble-algorithms-for-machine-learning/. Accessed 2023-010-04.

Cao, G., Han, D., Song, X., 2013. Evaluating actural evapotraspiration and impacts of groundwtaer storage caneg in the North China Plain. J. Hydrol. Process. 28, 1797–1808. https://doi.org/10.1002/hyp.9732.

Chen, L., He, Q., Liu, K., Li, J., Jing, C., 2019. Downscaling of GRACE-derived groundwater storage based on the random forest model. Remote Sens. 11, 2979. https://doi.org/10.3390/rs11242979.

Chen, X., Song, J., Wang, W., 2010. Spatial variability of specific yield and vertical hydraulic conductivity in a highly permeable alluvial aquifer. J. Hydrol. 388, 3–4. https://doi.org/10.1016/j.jhydrol.2010.05.017.

Chen, J.L., Wilson, C.R., Tapley, B.D., Save, H., Cretaux, J.F., 2017. Long-term and seasonal Caspian Sea level change from satellite gravity and altimeter measurements. J. Geophys. Res. Solid Earth 122 (3), 2274–2290. https://doi.org/10.1002/2016JB013595.

Crop Estimates Consortium., 2021. Field Crop Boundary (FCB) data layer (Gauteng province), 2021. Pretoria. Department of Agriculture, Land Reform and Rural Development.

De Bruin K., Rademan Z., Towers L. 2023. Guidance document for management of a groundwater scheme. Water Research Commission (WRC) Report No. TT 906/22. ISBN 978-0-6392-0374-4. March 2023.

Du Plessis, J.A., Kibii, J.K., 2021. Applicability of CHIRPS-based satellite rainfall estimates for South Africa Article. J. South Afr. Inst. Civ. Eng. 63 (3) https://doi.org/10.17159/2309-8775/2021/v63n3a4.

Eriksson, P.G., Altermann, W., Hartzer, F.J., 2009. The Transvaal Supergroup and its precursors. In: Johnson, M.R.;, Anhaeuser, C.R., Thomas, R.J. (Eds.), The Geology of South Africa. The Geological Society of South Africa, Johannesburg, pp. 237–260.

Feng, W., Zhong, M., Lemoine, J., Biancale, R., Hsu, H., Xia, J., 2013. Evaluation of groundwater depletion in North China using the Gravity Recovery and Climate Experiment (GRACE) data and ground-based measurements. Water Resour. Res. 49, 2110–2118. https://doi.org/10.1002/wrcr.20192.

Funk, C., Peterson, P., Landsfeld, M., Pedreros, D., Verdin, J., Shukla, S., et al., 2015. The climate hazards infrared precipitation with stations: a new environmental record for monitoring extremes. Sci. Data 2 (1), 21. https://doi.org/10.1038/sdata.2015.66.

Gaffoor, Z., Gritzman, A., Pietersen, K., Jovanovic, N., Bagula, A., Kanyerere, T., 2022. An autoregressive machine learning approach to forecast high-resolution groundwater-level anomalies in the Ramotswa/North West/Gauteng dolomite aquifers of Southern Africa. Hydrogeol. J. 30, 575–600. https://doi.org/10.1007/s10040-021-02439-4.

Gaffoor, Z., Pietersen, K., Jovanovic, N., Bagula, A., Kanyerere, T., 2020. Big data analytics and its role to support groundwater management in the Southern Africa development community, 2796 Water (12), 1–28. https://doi.org/10.3390/w12102796.

Gemitzi, A., Koutsias, N., Lakshmi, V.A., 2021. Spatial downscaling methodology for GRACE total water storage anomalies using GPM IMERG precipitation estimates. Remote Sens. 13, 5149. https://doi.org/10.3390/rs13245149.

Hoare J. 2023. How is Splitting Decided for Decision Trees?. Advanced Analysis. Machine Learning. https://www.displayr.com/how-is-splitting-decided-for-decision-trees/ Accessed 2023-11-04.

Holland M., Wiegmans F. 2009. Geohydrology Guideline Development: Implementation of Dolomite Guideline – Phase 1: Activity 19 & 28. Department of Water Affairs. Project No. 14/14/5/2.

Jain, K., Kaushik, K., Gupta, S.K., Mahajan, S., Kadry, S., 2023. Machine learning-based predictive modelling for the enhancement of wine quality. Oct 9 Sci. Rep. 13 (1), 17042. https://doi.org/10.1038/s41598-023-44111-9. PMID: 37814043; PMCID: PMC10562461.

Joseph J.E., Akinrotimi O.O., Rao KPC, Ramaraj A. 2020. The usefulness of gridded climate data products in characterising climate variability and assessing crop production. doi:10.13140/RG.2.2.27548.31367.

Karimi, P., Bastiaanssen, W.G.M., 2015. Spatial evapotranspiration, rainfall and land use data in water accounting - Part 1: review of the accuracy of the remote sensing data. Hydrol. Earth Syst. Sci. 19 (1), 507–532. https://doi.org/10.5194/hess-19-507-2015.

Kenda, K., Cerin, M., Bogataj, M., Senozetnik, M., Klemen, K., Pergar, P., Laspidou, C., Mladenic, D., 2018. Groundwater modelling with machine learning techniques: Ljubljana polje aquifer. Multidiscip. Digit. Publ. Inst. Proc. 2 (11), 697. https://doi.org/10.3390/proceedings2110697.

Keyser N. 1986. 1:250 000 Geological Map of the Wes Rand, 2626. South African Committee for Stratigraphy, Council for Geoscience, Pretoria. https://maps.geoscience.org.za/portal/home/item.html?id=a5cf6f95652d446e8dcd7bc7ec11340c.

Kotchoni, D.O.V., Vouillamoz, J.M., Lawson, F.M.A., et al., 2019. Relationships between rainfall and groundwater recharge in seasonally humid Benin: a comparative analysis of long-term hydrographs in sedimentary and crystalline aquifers. Hydrogeol. J. 27, 447–457. https://doi.org/10.1007/s10040-018-1806-2.

Kuhn C.M. 1986. Geohydrological investigation of the western and central Steenkoppies compartment. Technical Report Gh3446. Directorate Geohydrology. Department of Water Affairs and Forestry, Pretoria.

Le Roux, B., van der Laan, M., Vahrmeijer, T., Annandale, J.G., Bristow, K.L., 2016. Estimating water footprints of vegetable crops: influence of growing season, solar radiation data and functional unit. *Water* 2016 8, 473. https://doi.org/10.3390/w8100473.

Li, B., Rodell, M., Kumar, S., Beaudoing, H.K., Getiran, A., Zaitchik, B.F., et al., 2019. Global GRACE data assimilation for groundwater and drought monitoring: advances and challenges. Water Resour. Res. 55, 7564–7586. https://doi.org/10.1029/2018WR024618.

Liesch, T., Ohmer, M., 2016. Comparison of GRACE data and groundwater levels for the assessment of groundwater depletion in Jordan. Hydrol. J. 24, 1547–1563. https://doi.org/10.1007/s10040-016-1416-9.

Meyer R. 2014. Hydrogeology of Groundwater Region 10: The Karst Belt. Water Research Commission (WRC) Report No. TT 553/14. ISBN 978-1-4312-0391-8.

Milewski, A.M., Thomas, M.B., Seyoum, W.M., Rasmussen, T.C., 2019. Spatial downscaling of GRACE TWSA data to identify spatiotemporal groundwater level trends in the Upper Floridan Aquifer, Georgia, USA. Remote Sens. 11, 2756. https://doi.org/10.3390/rs11232756.
Moiwo, J.P., Yang, Y., Han, S., Lu, W., Yan, N., Wu, B., 2011. A method for estimating soil moisture storage in regions under water stress and storage depletion: a case study of Hai River Basin, North China. Hydrol. Process. 25, 2275–2287. https://doi.org/10.1002/hyp.7991.
Monteith, J.L., 1965. Evaporation and environment. Symp. Soc. Exp. Biol. 19, 205–234.
Moore, J.M., Tsikos, H., Polteau, S., 2001. Deconstructing the Transvaal Supergroup, South Africa: implications for Palaeoproterozoic palaeoclimate models (Elsevier). *J. Afr. Earth Sci.* 2001 33, 437–444. https://doi.org/10.1016/S0899-5362(01)00084-7.
Mu, Q., Heinsch, F.S., Zhao, M., Running, S.W., 2007. Development of a global evapotranspiration algorithm based on MODIS and global meteorology data. Remote Sens. Environ. 111, 519–536. https://doi.org/10.1016/j.rse.2007.04.015.
Mu, Q., Zhao, M., Running, S.W., 2011. Improvements to a MODIS global terrestrial evapotranspiration algorithm. Remote Sens. Environ. 115, 1781–1800. https://doi.org/10.1016/j.rse.2011.02.019.
Rahaman, M.M., Thakur, B., Kalra, A., Li, R., Maheshwari, P., 2019. Estimating high-resolution groundwater storage from GRACE: a random forest approach. Environments 6, 63. https://doi.org/10.3390/environments6060063.
Ramjeawon, M., Demlie, M., Toucher, M., 2022. Analyses of groundwater storage change using GRACE satellite data in the Usutu-Mhlatuze drainage region, north-eastern South Africa. J. Hydrol.: Reg. Stud. 42, 101118 https://doi.org/10.1016/j.ejrh.2022.101118.
Rodell, M., Chen, J., Kato, H., Famiglietti, J.S., Nigro, J., Wilson, C.R., 2007. Estimating groundwater storage changes in the Mississippi River basin (USA) using GRACE. Hydrogeol. J. 15 (1), 159–166. https://doi.org/10.1007/s10040-006-0103-7.
Rose, M.D., Fidelibus, C., Martano, P., 2018. Assessment of specific yield in karstified fractured rock through the water-budget method. Geosciences 8 (9), 344. https://doi.org/10.3390/geosciences8090344.
Rui H., Beaudoing H., Loeser C. 2022. README Document for NASA GLDAS Version 2 Data Products. National Aeronautics and Space Administration (NASA) and Goddard Earth Sciences Data and Information Services Centre (GES DISC).
Rukundo, E., Doğan, A., 2019. Dominant influencing factors of groundwater recharge spatial patterns in Ergene River catchment, Turkey. Water 11, 653. https://doi.org/10.3390/w11040653.
Running S., Mu Q., Zhao M. 2021. MODIS/Terra Net Evapotranspiration 8-Day L4 Global 500m SIN Grid V061. Distributed by NASA EOSDIS Land Processes DAAC, https://doi.org/10.5067/MODIS/MOD16A2.061. Accessed 2023-07-04.
Sabzehee, F., Amiri-Simkooei, A.R., Iran-Pour, S., Vishwakarme, B.D., Kerachian, R., 2023. Enhancing spatial resolution of GRACE-derived groundwater storage anomalies in Urmia catchment using machine learning downscaling methods. J. Environ. Manag. 330, 117180 https://doi.org/10.1016/j.jenvman.2022.117180.
Sadath P.V.R., Kartheeshware M.R., Elango L. 2023. Sustainable groundwater management under global climate change: mitigation and adaptation measures. In: Li, P., Elumalai, V. (eds) Recent Advances in Environmental Sustainability. EESIWC 2021. *Environmental Earth Sciences*. Springer, Cham. https://doi.org/10.1007/978-3-031-34783-2_10.
Sahour H. 2020. Statistical Downscaling Techniques to Enhance the Spatial Resolution of the Grace Satellite Data and to Fill Temporal Gaps. Dissertations. 3634. https://scholarworks.wmich.edu/dissertations/3634.
Save, H., Bettadpur, S., Tapley, B.D., 2016. High-resolution CSR GRACE RL05 mascons. J. Geophys. Res. Solid Earth 121 (10), 7547–7569. https://doi.org/10.1002/2016JB013007.
Sen, Z., 2015. Chapter 6- Groundwater Management. Pract. Appl. Hydrogeol. 341–397. https://doi.org/10.1016/B978-0-12-800075-5.00006-6.
Seyoum, W.M., Kwon, D., Milewski, M., 2019. Downscaling GRACE TWSA data into high-resolution groundwater level anomaly using machine learning-based models in a glacial aquifer system. Remote Sens 11, 824. https://doi.org/10.3390/rs11070824.
Shelestov, A., Lavreniuk, M., Kussul, N., Novikov, A., Skakun, S., 2017. Exploring google earth engine platform for big data processing: classification of multi-temporal satellite imagery for crop classification. February 2017 Front. Earth Sci. Vol 5 (No. 17). https://doi.org/10.3389/feart.2017.00017.
Srivastava R., Kumar S., Kumar B. 2023. Classification model of machine learning for medical data analysis. Chapter 7. *Statistical Modeling in Machine Learning*. Academic Press, Pages 111-132 ISBN 9780323917766.
Strassberg, G., Scanlon, B.R., Rodell, M., 2007. Comparison of seasonal terrestrial water storage variations from GRACE with groundwater-level measurements from the High Plains Aquifer (USA). Geophys. Res. Lett. 34. L14402, doi:10.1029/2007GL030139, 2007.
Swenson, S., Wahr, J., 2002. Methods for inferring regional surface-mass anomalies from Gravity Recovery and Climate Experiment (GRACE) measurements of time-variable gravity. J. Geophys. Res. Solid Earth 107 (B9). https://doi.org/10.1029/2001JB000576. ETG-3.
Twine, T.E., Kustas, W.P., Norman, J.M., Cook, D.R., Houser, P.R., Meyers, T.P., Prueger, J.H., Starks, P.J., Wesely, M.L., 2000. Correcting eddy-covariance flux underestimates over a grassland. Agric. Meteorol. 103, 279–300. https://doi.org/10.1016/S0168-1923(00)00123-4.
Vahrmeijer, J.T., Annandale, J.G., Bristow, K.L., Steyn, J.M., Holland, M., 2013. Drought as a catalyst for change: A case study of the Steenkoppies Dolomite Aquifer. In: Schwabe, K., Albiac, J., Connor, J., Hassan, R., Meza Gonzalez, L. (Eds.), Drought in arid and semi-arid regions: A multi-disciplinary and cross-country perspective. Springer Publications, Dordrecht, pp. 251–268.
Vishwakarma, B.D., Devaraju, B., Sneeuw, N., 2018. What Is the Spatial Resolution of GRACE Satellite Products for Hydrology?, 2018 Remote Sens 10, 852. https://doi.org/10.3390/rs10060852.
Vishwakarma, B.D., Zhang, J., Sneeuw, N., 2021. Downscaling GRaCE total water storage change using partial least squares regression. Sci. Data 8, 95. https://doi.org/10.1038/s41597-021-00862-6.
Wiegmans F.E., Holland M., Janse Van Rensburg H. 2013. Groundwater Resource Directed Measures for Maloney's Eye Catchment. Report emanates from a project entitled Groundwater Resource Directed Measures for Maloney's Eye Catchment. Water Research Commission Project No. K8/970.
Yan, X., Zhang, B., Yao, Y., Yin, J., Wang, H., Ran, Q., 2022. Jointly using the GLDAS-2.2 model and GRACE to study the severe Yangtze flooding of 2020. J. Hydrol. 610 (3-4), 127927 https://doi.org/10.1016/j.jhydrol.2022.127927.
Yeh, P.J.F., Swenson, S., Famiglietti, J., Rodell, M., 2006. Remote sensing of groundwater storage changes in Illinois using the Gravity Recovery and Climate Experiment (GRACE. Water Resour. Res. 42 (12) https://doi.org/10.1029/2006WR005374.
Yin, W., Hu, L., Zhang, M., Wang, J., Han, S.C., 2018. Statistical downscaling of GRACE-derived groundwater storage using ET data in the North Chine Plain. J. Geophys. Res.: Atmospheres 123, 5973–5987. https://doi.org/10.1029/2017JD027468.
Yiu T. 2019. Understanding Random Forest: How the Algorithm Works and Why it Is So Effective. Towards Data Science. https://towardsdatascience.com/understanding-random-forest-58381e0602d2.
Yu, S., Ding, H., Zeng, Y., 2022. Evaluating water-yield property of karst aquifer based on the AHP and CV. Sci. Rep. 12, 3308. https://doi.org/10.1038/s41598-022-07244-x.